The interaction between the turbulence and gravity wave observed in the middle stratosphere based on the round-trip intelligent sounding system

Zheng Sheng[1], Yang He[1], and Mingyuan He[1]

[1]National University of Defense Technology

November 24, 2022

Abstract

Abstract Based on the round-trip intelligent sounding system, we used the structure function and spectrum analysis method to analyze the interaction between the small-scale gravity wave and turbulence in the middle stratosphere. The result showed that the generation of turbulence was closely related to the Kelvin-Helmholtz(KH) billows. An upscale energy cascade occurred on the spatial scale of KH billows, while a downscale energy cascade occurred on a larger spatial scale (gravity wave scale), which resulted in the breaking of the gravity wave and turbulence. Obvious two-dimensional turbulence that the inverse energy cascade in 2D exists simultaneously with a direct enstrophy cascade to the small scales was found, which is considered to be the first-hand observation result of relevant height.

The interaction between the turbulence and gravity wave observed in the middle stratosphere based on the round-trip intelligent sounding system

Yang He[1], Zheng Sheng[1,2], Mingyuan He[1],

[1]College of Meteorology and Oceanography, National University of Defense Technology, Changsha, 410073, China

[2] Collaborative Innovation Center on Forecast and Evaluation of Meteorological Disasters, Nanjing University of Information Science and Technology, Nanjing 210094, China

Corresponding author: Zheng Sheng (19994035@sina.com)

Key Points:

- The two-dimensional turbulence is found with bidirectional **e**nergy transmission.
- KH billows are considered to be an important factor in the excitation of turbulence.
- Convergence and divergence on different scales causes instability within the wave.

Abstract

Based on the round-trip intelligent sounding system, we used the structure function and spectrum analysis method to analyze the interaction between the small-scale gravity wave and turbulence in the middle stratosphere. The result showed that the generation of turbulence was closely related to the Kelvin-Helmholtz(KH) billows. An upscale energy cascade occurred on the spatial scale of KH billows, while a downscale energy cascade occurred on a larger spatial scale (gravity wave scale), which resulted in the breaking of the gravity wave and turbulence. Obvious two-dimensional turbulence that the inverse energy cascade in 2D exists simultaneously with a direct enstrophy cascade to the small scales was found, which is considered to be the first-hand observation result of relevant height.

1 Introduction

Gravity wave(GW) is an important atmospheric disturbance feature in the middle atmosphere (10-110 km) and plays a pivotal role in atmospheric circulation, structure, and dynamic evolution (Fritts & Alexander, 2012). As the atmospheric density decreases, the amplitude of GW increases during the uploading process, and finally breaks once it reaches saturation. The entire GW evolution process is accompanied by energy propagation and dissipation, and its effect on the background field(Fritts & Rastogi, 1985). The breaking of GW can lead to the generation of turbulence, and the connection between GW and turbulence has become a focus in recent years. Limited by detection methods, in-situ, long-time, and high-frequency observations for turbulence and GW in stratosphere are currently lacking.

The work presented in this paper aims to fill the gap in observation experimental data from in situ measurements for interaction between the turbulence and gravity wave of scales in the range from several meters to several kilometers in the middle stratosphere. At the same time, considering that the transmission mechanism of energy is mainly studied under different numerical experimental systems(Byrne et al., 2011; Deusebio et al., 2014; Kurien et al., 2006; Lindborg, 2007), observations about the energy cascade of turbulent systems in the stratosphere are very scarce and our results can provide a valuable reference. The detection system includes three-stages of "rising, flat-floating and falling", here we mainly use the data obtained during its flat-floating phase. System's 2-s sampling rate makes it possible to characterize the main features of the meso-scale, micro-scale and weather-scale dynamics in the corresponding atmospheric area. In this paper, three sets of experimental data obtained in Wuhan and Anqing were selected and the corresponding heights of the three sets of data in the flat-floating phase are 25.3, 28.8 and 27.5 km respectively (hereinafter referred to as WH, AQ1 and AQ2 respectively).

This article will discuss the following questions: What is the transmission mechanism of energy in the middle stratosphere, will the turbulence affect the direction of the cascade? How is the generation of turbulence and GWs connected at this height? Can the above phenomenon in the middle stratosphere be explained well by structure function or spectrum analysis method? In order to effectively describe small-scale structures, we will use both spectral analysis and structure function methods. Among them, the spectrum analysis method can intuitively display the energy component of the corresponding wavenumber region, while the third-order structure function can indicate the direction of the energy cascade, with the separation distance directly corresponding to the measurement speed between two points, which is more straightforward(Lindborg, 1999). To further describe the quantitative characteristics of waves and turbulence, multi-order structure

functions and singularity measurement were used to analyze the multifractal process (A. Davis et al., 1994; Anthony Davis et al., 1996; Marshak et al., 1997), thus Hurst parameters and intermittent parameters were introduced.

2 Materials and Methods

2.1 Data

The round-trip intelligent radiosonde system carries the Beidou positioning module and the meteorological sensor module. Assuming that the radiosonde performs quasi-Lagrangian motion with the background wind field, we can calculate the wind speed and wind direction according to the latitude and longitude coordinates, and convert it into a topocentric terrestrial coordinate system. The real-time position of the radiosonde is represented by (X, Y, Z). The sensor module includes temperature, air pressure, and humidity sensors. Compared with aircraft detection, the quasi-Lagrangian motion observed by balloons is more conducive to the analysis of the disturbance caused by GWs (Hertzog et al., 2002; Hertzog & Vial, 2001). For flat-floating phase, considering that the balloon trajectory is affected by the background wind field, we decompose it into the meridional and latitudinal directions and re-interpolate according to the average step size. According to the characteristics of the data, WH and AQ1 are decomposed according to the meridian direction, with an average step size of 12 m and 11 m, and AQ2 is decomposed according to the latitude direction, with an average step size of 16 m. The direction of the arrow is consistent with the direction of the separation distance r, that is, the direction of the longitudinal component of the horizontal velocity. The trajectory lengths of the three groups after decomposition are 90.3 km, 29.0 km and 53.6 km, respectively.

2.2 Spectrum and structure function analysis

Many results indicate that in high wavenumber regions, the spectral amplitude and slope have a wide range(Dewan & Good, 1986; Nastrom et al., 1984; Nastrom & Gage, 1985; Smith et al., 1987). For planet-scale waves, the spectral slope can reach -3 or higher. And for smaller-scale waves, the slope will decrease. Considering that Kolmogorov's theory predicts that the law of -5/3 slope will be followed in the turbulent inertia region (Kolmogorov, 1991), it is reasonable for the spectral slope to be between -1 and -3(Cho & Lindborg, 2001). For any non-stationary, self-similar process, the general power law can be written as:

$$E(k) \propto k^{-\beta} \quad \text{where} \quad 1 \le \beta \le 3 \tag{1}$$

presuming transition in middle stratosphere is within a thin layer(Benavides & Alexakis, 2017), the third-order structure function for two-dimensional turbulence is defined as (diagonal part):

$$S_3(r) = \left\langle \left[\delta u_L(r) \right]^3 \right\rangle + \left\langle \delta u_L(r) [\delta u_T(r)]^2 \right\rangle \tag{2}$$

Where $\langle . \rangle$ is the ensemble average and r is the separation distance along the longitudinal

direction. u_L and u_T represent the velocity components parallel and perpendicular to the separation distance r respectively (the direction of the arrow in Figure 2 represents the separation distance), thus δu_L and δu_T can be written as:

$$\begin{cases} \delta u_L(x,r) = u_L(x+r) - u_L(x) \\ \delta u_T(x,r) = u_T(x+r) - u_T(x) \end{cases} \tag{3}$$

2.3 Multi-order structure function analysis and singular measure

In order to further obtain the specific characteristics of atmospheric disturbance, we choose Hurst index and intermittent parameter for quantitative description. For the q-order structure function,

$$S_q(r) = \left\langle \left| u(x+r) - u(x) \right|^q \right\rangle = \left\langle \left| \delta u(r) \right|^q \right\rangle \tag{4}$$

Assuming that $\delta u(r;x)$ does not depend on position x, then $\left\langle \left| \delta u(r;x) \right|^q \right\rangle = \left\langle \left| \delta u(r) \right|^q \right\rangle$. Assuming that the process of $u(x)$ is scale-invariant and self-similar, it can be scaled to:

$$S_q(r) = C_q r^{\zeta(q)} \quad \text{where} \quad q \geq 0 \tag{5}$$

Where C_q is a proportional constant and $\zeta(q)$ is a function that depends on q. A set of scale parameters with different q values can be defined as the following monotone, non-increasing function(Frisch, 1991; Marshak et al., 1997):

$$H(q) = \frac{\zeta(q)}{q} \tag{6}$$

According to the conversion law (Monin & Yaglom, 1975), it can be related to the general spectral power law:

$$1 < \beta = \zeta(2) + 1 = 2H(2) + 1 < 3 \tag{7}$$

We generally choose H_1 as the Hurst index to represent the roughness of the data series, where $0 < H_1 = H(1) = \zeta(1) < 1$. The larger the value of H_1, the smoother the data series, indicating that the intensity of atmospheric fluctuations is weaker, and vice versa. A η scale gradient field normalized by the average value is defined:

$$\varepsilon(\eta;x)=\frac{\left|\delta u_L(x,\eta)\right|^2}{\left\langle\left|\delta u_L(x,\eta)\right|^2\right\rangle},\ 0\le x<L-\eta, \tag{8}$$

Where L is the maximum data length and η is four times the Nyquist wavelength. Taking $\varepsilon(\eta;x)$ as the minimum unit quantity, various measure $\varepsilon(\eta;x)$ over scale r can be obtained by spatially averaging:

$$\varepsilon(r;x)=\frac{1}{r}\int_x^{x+r}\varepsilon(\eta;x')dx',\quad \eta\le x\le L-r. \tag{9}$$

The q-order measurement meets the following relationship:

$$\left\langle\varepsilon(r)^q\right\rangle\propto r^{-K(q)},\quad q\ge 0. \tag{10}$$

According to the variation of $\left\langle\varepsilon(r;x)^q\right\rangle$ with r, the slope is fitted by linear regression, and $K(q)$ can be obtained. Then the concept of "generalized dimension" is introduced (Grassberger, 1983; Hentschel & Procaccia, 1983):

$$D(q)=1-C(q)=1-\frac{K(q)}{q-1} \tag{11}$$

Where $C(q)=\frac{K(q)}{q-1}$ represents the hierarchy of the index. Consistent with the idea of defining the Hurst index, here we use the "information dimension" $D(1)$ (Carreras et al., 2000) to represent the physical characteristics of fluctuations. C_1 is selected as intermittent parameter, reflecting the degree of singularity of the fluctuation:

$$C_1=C(1)=1-D(1)=1-\lim_{q\to 1}\frac{K(q)}{q-1}=K'(1) \tag{12}$$

3 Results and discussion

3.1 Third-order structure function

Firstly, the third-order structure function $S_3(r)$ is calculated according to the method in section 2, where the separation distance $r=l\times 2^n$, $n=0,1...,N$. N is determined by the maximum data length. The results are shown in Figure 1 (left panel). The black curve represents $S_3(r)$ from the entire data length, while the purple curve and the cyan curve represent the first half and the second half of the entire data series, respectively. The drawn third-order structure functions are defined as

absolute values, where the red dots represent negative values and the blue dots represent positive values. The reference slopes r, r^2, and r^3 are also added. In the GW sub-range, $S_3(r)$ follows the r^2 slope when turbulence occurs or the r^3 slope without turbulence activity. According to this criterion, we observed obvious turbulence activity from the WH data. Both the cyan curve and the black curve clearly follow the r slope region, indicating that the obvious turbulent activity mainly occurs in the second half of the data. According to linear regression, we can see that the turbulence scale can reach between 200-300 m. At the same time, in the GW sub-range, both the black curve and the cyan curve follow the r^2 slope, while the purple curve is more inclined to the r^3 slope. For the data of AQ1 and AQ2, no turbulence is observed within the range of data resolution.

Different from Lu's result(Lu & Koch, 2008), as for the direction of energy cascade, we obtained more random results in the middle stratosphere, rather than showing the energy transfer process dominated by downscale cascade like the upper troposphere and lower stratosphere. In fact, for small and medium-scale disturbances, the upscale and downscale energy cascades can be dominated by one party or can exist simultaneously. For example, in the data of AQ1, the upscale energy cascade occurs in the first half of data over the whole space interval, while in the second half, all become downscale energy cascade. The entire data segment is dominated by upscale energy cascade. For the entire data of AQ2, the downscale energy cascade is dominated. For WH data, the first half of the data are upscale energy cascades. When turbulence occurs in the second half, we can see that it becomes a downscale energy cascade for r scale within 300 m, and the upscale energy cascade is retained at r scale from 300 m to 1 km. The direction of the energy cascade can be reflected by the sign of $S_3(r)$. According to $S_3(r) = \left\langle \delta u_L \left[(\delta u_L)^2 + (\delta u_T)^2 \right] \right\rangle$, when $S_3(r)$ is negative, δu_L<0, it means that the velocity is converging (or decelerating) on the spatial scale of r; when $S_3(r)$ is positive, δu_L > 0, it means that the velocity is divergent (or accelerating) on the spatial scale of r. When the data series contain only gravity wave and no turbulence activity (such as AQ1, AQ2), the $S_3(r)$ is basically all positive or negative in a wide range of spatial scales, indicating that the evolutionary trends of fluctuations from large scale to small are consistent and represent a dynamic stable state; when turbulence occurs in the series (such as WH), upscale energy cascade occurs in the mid-range spatial scale, while downscale energy cascade occurred in larger and smaller spatial scale. At this time, the internal wave activity is inconsistent on different scales. The inconsistency of the convergence and divergence of the velocity field at different spatial scales leads to the internal unstable state of the wave, which also causes turbulence. It is supposed that the upscale energy cascade can reflect the existence of KH billows, which can be generated by the overturn of GWs. However, the presence of KH billows will not necessarily cause the GWs to break and produce turbulence. In other words, the KH billows is generated after the GW overturning, and before the turbulence occurs (Liu et al., 2009). The WH data exactly reflects the breaking of GW caused by the KH billows, so that the energy cascade continues to decline throughout the turbulent inertia range and dissipates in the tail.

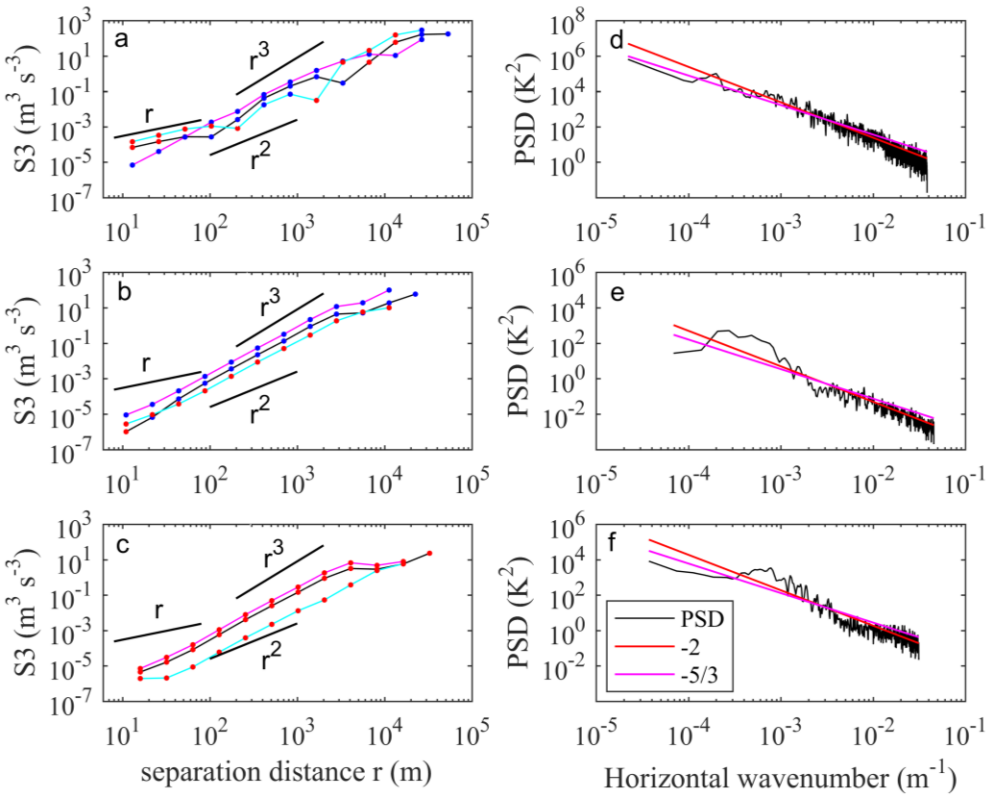

Figure 1. (a) The third-order structure function, (b) Horizontal wave number spectrum of the flat-floating stage from Wuhan. (c)-(d) The same as WH but for AQ1. (e)-(f) The same as WH but for AQ2.

3.2 Spectrum Analysis

Spectral analyses of potential temperature data are performed at the three levels and the power spectral densities(PSD) is obtained considering the potential temperature is used to describe the KH billows and is related to the evolution of GWs and turbulence (Klaassen & Peltier, 1985; Palmer et al., 1996). The 2π-normalized horizontal wavenumber spectrum in log-log coordinate from WH, AQ1 and AQ2 are shown in Figure 1 (right panel). The -5/3 slope and -2 slope are added for reference. An obvious feature is that the PSD of WH can better follow the -2 slope in a wider range of wavenumbers, while for AQ1 and AQ2, there is a "breaking point" where the spectral slope changes significantly (Cho et al., 1999), at 2×10^{-3} and 4×10^{-3} m^{-1}, respectively. For AQ1 and AQ2, in the region where the wavenumber is lower than the breaking point, the significantly increased slope can be considered as the spectral structure dominated by GWs, while for WH, the -2 slope in the whole wavenumber region is considered to be affected by the turbulence activity. According to the peak values of the PSDs of the three sets of data the corresponding characteristic wavenumbers can be found, we found that regardless of whether turbulence occurs, horizontal wavelengths in the range of several kilometers are still dominant. In the wavenumber region less than 10^{-4} m^{-1}, there is little wave interaction, and the PSD is mainly affected by the spectral characteristics of the wave source, which may be affected by planetary waves. However, in the wavelength range where waves and turbulence are related in this article, the dominant wavelength conforms to the wavelength range of KH waves, which belong to a two-dimensional structure

(Lesieur, 1993) and usually occur from a few hundred meters to several kilometers. Therefore, turbulence activity may be due to the effect of KH waves.

In order to further verify this point of view, we divided the WH data into nine groups according to the length of 10 km, the results are shown in Figure 2. In order to quantitatively describe the spectrum characteristics, we performed slope fitting in the range between 3×10^{-4} -0.01 m^{-1} and used the "center wavenumber" to calculate the spectral amplitude within the fitted interval (Dewan & Grossbard, 2000). In the figure, s is used to represent the slope, and A is the amplitude. Since we know that turbulence is generated in the second half of the data through the third-order structure function, we hope to verify this phenomenon through the evolution of spectral structure with time. Liu used numerical simulation to investigate the effect of KH waves on the average state of the atmosphere during the propagation of gravity waves (Liu et al., 2009), and found that before the KH waves are fully developed, the increased amplitude of unsaturated gravity waves will cause the increase of the spectral slope. When the KH wave is fully developed, the energy is transmitted from the large scale to the small scale, and the spectral slope decreases. It can be seen from Figure 2c-e that the spectral slope is gradually increasing (negative signs are ignored here), and the spectral amplitude of the gravity wave is also increasing. Before Figure 2f, the KH wave has reached saturation, after which the KH wave causes the breaking of the gravity wave, the spectrum amplitude and spectrum slope both decrease. The apparently lower spectral amplitude can be seen on Figure 2g-h, which may be due to the continuous downscale cascade process from the small-scale gravity wave to turbulence, which is eventually dissipated in the tail. The -1.52 slope in Figure 2h also further proves the generation of turbulence in the second half of the data, and the rapid decline of the power spectrum corresponding to the high wavenumber region can be considered as the dissipation of energy in the tail. Through the process of spectral analysis, we further verified the turbulence on the WH data observed from the third-order structure function, and we believe that this is due to the gravity wave breaking caused by the KH billows.

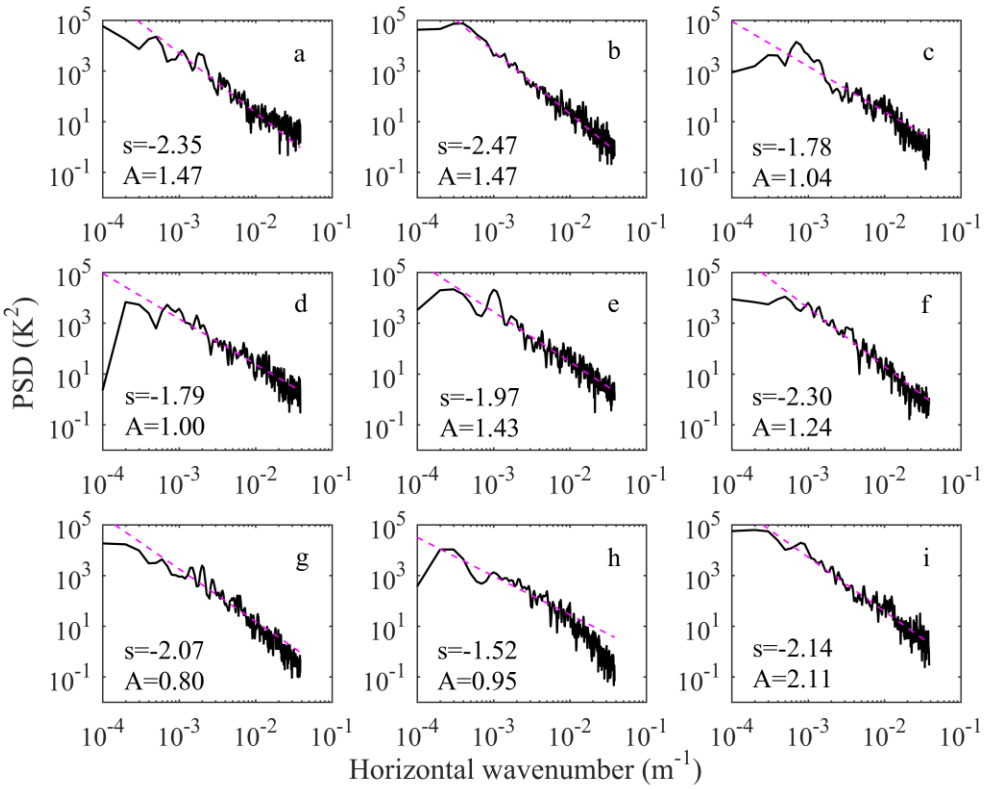

Figure 2. The horizontal wavenumber spectrum of WH calculated according to the data length of 10 km. (a)-(i) are the data segments in order from beginning to end. The purple dotted line represents the spectrum amplitude of the best linear fit, s represents the slope, and A ($\times 10^4$ K^2) represents the amplitude corresponding to the center wavenumber.

3.3 Multi-order structure function analysis and Hurst parameter

Using the of the three sets of flat-floating data from WH, AQ1 and AQ2, the multi-order structure function is calculated, as shown in Figure 3. It can be seen that as the order q increases, the curve can reflect more obvious variation and it is easier to distinguish between different scale ranges. Therefore, we focus on the curve of $q = 5$, which emphasizes the most intense events. Compared with WH, the fifth-order structure function of AQ1 and AQ2 have a clearer linear relationship, with $S_q(r)$ and r have a good linear fitting within the separation distances [40m,3km] and [60m, 2km], respectively. Considering the existence of turbulence on WH data, q =5 has some independent linear relationships in different scales. For example, in Figure 3a-c, there is an obvious scale breaking point (a significant change in the linear relationship for $S_q(r)$ and r, as the outer scale R.

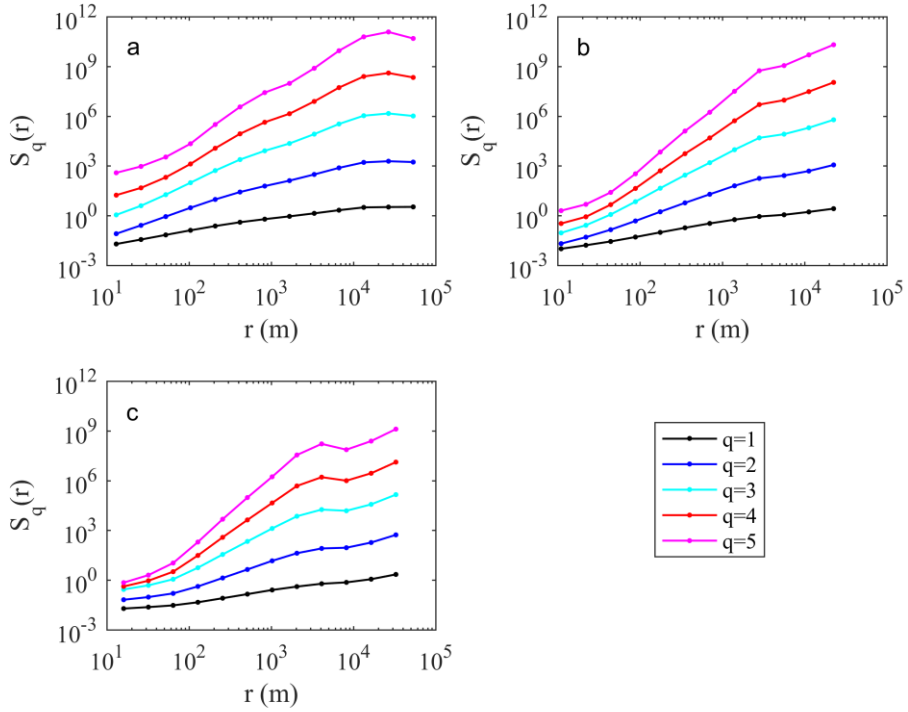

Figure 3. The multi-order structure function (q = 1,2,3,4,5) with the separation scale r as the calculated from the longitudinal component of the horizontal velocity from (a) WH, (b) AQ1 and (c) AQ2 in the flat-floating stage.

A linear regression is performed between the inner scale η and outer scale R in log-log coordinate to obtain $\zeta(q)$. The Hurst parameter $H_1 = \zeta(1)$ is obtained by least-squares linear fitting on the first-order structure function. Calculation of H_1 allows the straightforward identification of persistence, or long-time correlation, as well as the stationary/nonstationary and monofractal/multifractal nature of the data(Yu et al., 2003), with the range between 0-1. The larger the value, the smoother the data series. The Hurst parameters of WH, AQ1 and AQ2 are 0.67, 0.83 and 0.79 respectively. The WH segment has a smaller Hurst parameter due to strong GW and turbulence activity. $H_2 = \frac{\zeta(2)}{2}$ can be related to the power spectrum slope $-\beta$ by the conversion law of equation (10). The spectral slope $-\beta$ of WH, AQ1 and AQ2 fitted in Figure 4 are -2.21, -2.75 and -2.69, while the corresponding values of $\zeta(2)$ are 1.33, 1.71 and 1.67, respectively. It can be seen that the three sets of data satisfy the relationship "$\beta = 2H_2 + 1 = \zeta(2) + 1$" well, which also shows that structural function analysis is a supplement to the spectral analysis method, and it has a good consistency for the analysis of the disturbance information in the middle stratosphere.

3.4 Singular measures and intermittent parameter

Intermittent parameters are also used to describe the statistical characteristics of turbulence.

$K(q)$ can be obtained by linear fitting according to $\left\langle \varepsilon(r;x)^q \right\rangle$ and r between the inner scale η and outer scale R in log-log coordinate, as shown in equation (10), we use enough q (q = 0, 0.25, 0.5, ..., 5) to obtain sufficient $K(q)$, intermittent parameters can be obtained from the slope of the tangent line at q=1. It should be noted here that $K(0) = K(1) = 0$ needs to be satisfied when using this method to calculate C_1, which means that the data analyzed is a non-stationary random atmospheric process with stationary increment, and must satisfy the scale invariance within the interval [η, R](Marshak et al., 1997). Therefore, for the three-segment data, we need to carefully select the interval for slope fitting to eliminate the interference of the results caused by significant increments outside the outer scale. Figure 9a is the relationship between the multi-level singularity measure $\left\langle \varepsilon(r)^q \right\rangle$ and the spatial scale r in log-log coordinate, and Figure 9b is the variation of slope $K(q)$ with q, which is calculated according to Figure 9a. In Figure 9a, r starting from the first value greater than η, the interval for slope fitting corresponds to the interval satisfying the linear relationship in Figure 7a. Since turbulence and gravity waves co-exist in this data sequence, the intermittent parameters for turbulence and wave are calculated respectively within the fitting interval of $[\eta, R_t]$ and $[R_t, R_w]$. The C_1 calculated based on the slope of the purple curve represents turbulence, where C_1^t=0.20, and the C_1 calculated based on the slope of the blue curve represents gravity wave, where C_1^w=0.10. In the same way, the intermittent parameters of AQ1 and AQ2 are calculated and the results are shown in Figure 10 and Figure 11, with C_1=0.09 and C_1=0.07, respectively. It can be seen that when turbulent activity occurs, it is accompanied by a significantly increased intermittent parameter. To make Hurst parameter and intermittent parameters match, the WH data is further divided to calculate Hurst parameter as H_1^T=0.80 for the turbulence scale and H_1^w=0.61 for the gravity wave scale. The result seems to be contrary to our general perception that the gravity wave packet has a smoother motion than turbulence. However, it is consistent with the actual spectral structure (Figure 5h), that is, the turbulent inertia interval has a deeper spectral slope than the GW sub-range. Since the bidirectional energy transmission is found by third-order structure function, the inverse energy cascade in 2D exists simultaneously with a direct enstrophy cascade to the small scales, and the forward enstrophy cascade will lead to a smooth velocity field, getting a larger Hurst parameter(Biferale et al., 2013; Xie & Bühler, 2019).

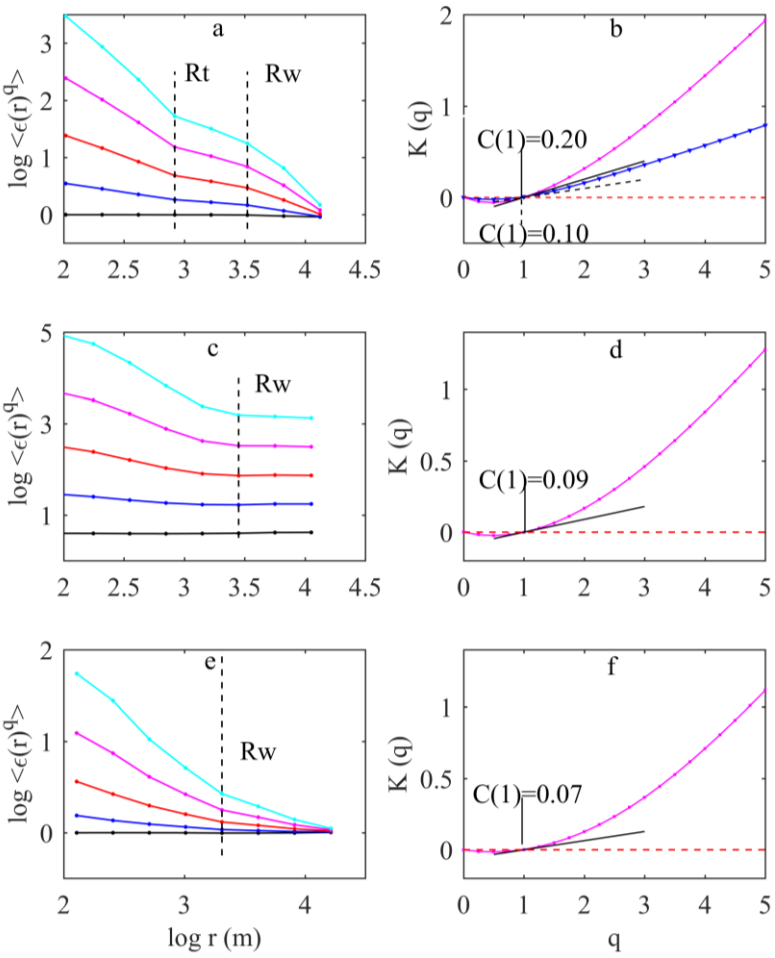

Figure 4. (a) The variation of multi-order singularity measure with spatial scale for WH data, (b) The variation of slope with order q for WH data. (c)-(d) The same as WH but for AQ1. (e)-(f) The same as WH but for AQ2. The red dotted line corresponds to $K(q)=0$, and the solid black line (dashed line) represents the tangent slope of the turbulent (gravity wave) area at $q=1$.

4 Conclusion and outlook

In this paper, the GWs and turbulence activity is observed in the middle stratosphere by in-situ, long-time, and high-frequency measurement. Using third-order structure function analysis, obvious turbulence activity was observed on WH data, which is generated in the second half of the data. In turbulent systems, the direction of energy transmission is an important concern. The results of this article show that it is different from the traditional isotropic two- and three-dimensional turbulence theory(Kolmogorov, 1941; Kraichnan, 1967), when turbulent activity occurs, energy transmission can be bidirectional, instead of just one party dominating.

Using spectrum analysis as a supplementary tool, this phenomenon has been further verified. By analyzing the variation trend of the spectral structure with time, we found that there is a KH billows evolution process in the first half of the WH data and the turbulence was observed in the second half of the data, which shows that only the activity of KH wave reaches a certain intensity,

will the turbulence be generated by the breaking of the gravity wave. In general, the results from structural function analysis and spectral analysis have a good consistency, and both show good results in atmospheric dynamics and energy analysis in the middle stratosphere.

By using Hurst parameter and intermittent parameter to quantitatively describe the signal characteristics of the data, the intensity of turbulence and gravity wave activities can be intuitively reflected. The connection of the two parameters can be used as an important diagnostic method for analyzing gravity wave and turbulence. Our results show obvious two-dimensional turbulence that the inverse energy cascade exists simultaneously with a direct enstrophy cascade to the small scales, which is completely different from the three-dimensional turbulent in the upper troposphere and lower stratosphere(Lu & Koch, 2008). Two-dimensional turbulence with bidirectional energy transmission is proved from the first-hand observation results in the middle stratosphere. Considering that a large number of stratospheric data can be obtained after the later expansion of this type of new sounding system, which can provide a reference from the observation data for the relevant models and parameterization schemes, it will have a good application prospect in mapping of turbulence and GWs in the bifractal parameter space.

Acknowledgments, Samples, and Data

This work was supported by the National Natural Science Foundation of China (Grant no. 41875045). This work was also partly supported by the National Natural Science Foundation of China (Grant no. 41576171). Thanks for the support provided by the experimental project of round-trip intelligent sounding system. Additionally, helpful comments by the specific anonymous reviewer are gratefully acknowledged. Data archiving is underway in 4TU.ResearchData (http://doi.org/10.4121/uuid:38f8105a-5f70-4c6b-806b-e1301d240f73).

References

Benavides, S. J., & Alexakis, A. (2017). Critical transitions in thin layer turbulence. *Journal of Fluid Mechanics*, *822*, 364–385. https://doi.org/10.1017/jfm.2017.293

Biferale, L., Musacchio, S., & Toschi, F. (2013). Split energy-helicity cascades in three-dimensional homogeneous and isotropic turbulence. *Journal of Fluid Mechanics*, *730*, 309–327. https://doi.org/10.1017/jfm.2013.349

Byrne, D., Xia, H., & Shats, M. (2011). Robust inverse energy cascade and turbulence structure in three-dimensional layers of fluid. *Physics of Fluids*, *23*, 095109. https://doi.org/10.1063/1.3638620

Carreras, B. A., Lynch, V. E., Newman, D. E., Balbín, R., Bleuel, J., Pedrosa, M. A., et al. (2000). Intermittency of plasma edge fluctuation data: Multifracial analysis. *Physics of Plasmas*, *8*, 3278–3287. https://doi.org/10.1063/1.874193

Cho, J. Y. N., & Lindborg, E. (2001). Horizontal velocity structure functions in the upper troposphere and lower stratosphere 1. Observations. *Journal of Geophysical Research Atmospheres*, *106*(D10), 10223–10232. https://doi.org/10.1029/2000JD900814

Cho, J. Y. N., Zhu, Y., Newell, R. E., Anderson, B. E., Barrick, J. D., Gregory, G. L., et al. (1999). Horizontal wavenumber spectra of winds, temperature, and trace gases during the

Pacific Exploratory Missions: 1. Climatology. *Journal of Geophysical Research Atmospheres*, *104*, 5697–5716. https://doi.org/10.1029/98JD01825

Davis, A., Marshak, A., Wiscombe, W., & Cahalan, R. (1994). Multifractal characterizations of nonstationarity and intermittency in geophysical fields: observed, retrieved, or simulated. *Journal of Geophysical Research*, *99*, 8055–8072. https://doi.org/10.1029/94JD00219

Davis, Anthony, Marshak, A., Wiscombe, W., & Cahalan, R. (1996). Scale invariance of liquid water distributions in marine stratocumulus. Part I: Spectral properties and stationarity issues. *Journal of the Atmospheric Sciences*, *53*(11), 1538–1558. https://doi.org/10.1175/1520-0469(1996)053<1538:SIOLWD>2.0.CO;2

Deusebio, E., Augier, P., & Lindborg, E. (2014). Third-order structure functions in rotating and stratified turbulence: A comparison between numerical, analytical and observational results. *Journal of Fluid Mechanics*, *755*, 294–313. https://doi.org/10.1017/jfm.2014.414

Dewan, E. M., & Good, R. E. (1986). Saturation and the "universal" spectrum for vertical profiles of horizontal scalar winds in the atmosphere. *Journal of Geophysical Research*, *91*, 2742–2748. https://doi.org/10.1029/JD091iD02p02742

Dewan, E. M., & Grossbard, N. (2000). Power spectral artifacts in published balloon data and implications regarding saturated gravity wave theories. *Journal of Geophysical Research Atmospheres*, *105*(D4), 4667–4683. https://doi.org/10.1029/1999JD901108

Frisch, U. (1991). From global scaling, à la Kolmogorov, to local multifractal scaling in fully developed turbulence. *Proceedings of the Royal Society of London. Series A: Mathematical and Physical Sciences*, *A434*, 89–99. https://doi.org/10.1098/rspa.1991.0082

Fritts, D. C., & Alexander, M. J. (2012). Gravity wave dynamics and effects in the middle atmosphere. *Reviews of Geophysics*, *50*(3). https://doi.org/10.1029/2012rg000409

Fritts, D. C., & Rastogi, P. K. (1985). Convective and dynamical instabilities due to gravity wave motions in the lower and middle atmosphere: Theory and observations. *Radio Science*, *20*, 1247–1277. https://doi.org/10.1029/RS020i006p01247

Grassberger, P. (1983). Generalized dimensions of strange attractors. *Physics Letters A*, *97*, 227–330. https://doi.org/10.1016/0375-9601(83)90753-3

Hentschel, H. G. E., & Procaccia, I. (1983). The infinite number of generalized dimensions of fractals and strange attractors. *Physica D: Nonlinear Phenomena*, *8*, 435–444. https://doi.org/10.1016/0167-2789(83)90235-X

Hertzog, A., & Vial, F. (2001). A study of the dynamics of the equatorial lower stratosphere by use of ultra-long-duration balloons: 2. Gravity waves. *Journal of Geophysical Research Atmospheres*, *106*(D19), 22745–22761. https://doi.org/10.1029/2000JD000242

Hertzog, A., Vial, F., Mechoso, C. R., Basdevant, C., & Cocquerez, P. (2002). Quasi-Lagrangian measurements in the lower stratospere reveal an energy peak associated with near-inertial waves Quasi-Lagrangian measurements in the lower stratosphere reveal an energy peak associated with near-inertial waves, (April). https://doi.org/10.1029/2001GL014083

Klaassen, G. P., & Peltier, W. R. (1985). Evolution of finite amplitude Kelvin-Helmholtz billows in two spatial dimensions. *Journal of the Atmospheric Sciences*, *42*, 1321–1339. https://doi.org/10.1175/1520-0469(1985)042<1321:EOFAKB>2.0.CO;2

Kolmogorov, A. (1941). Dissipation of energy in the locally isotropic turbulence. *Dokl. Akad. Nauk SSSR*, *32*, 16–18. https://doi.org/10.1098/rspa.1991.0076

Kraichnan, R. H. (1967). Inertial ranges in two-dimensional turbulence. *Physics of Fluids*, *10*, 1417–1423. https://doi.org/10.1063/1.1762301

Kurien, S., Smith, L., & Wingate, B. (2006). On the two-point correlation of potential vorticity in rotating and stratified turbulence. *Journal of Fluid Mechanics*, *555*, 131–140. https://doi.org/10.1017/S0022112006009116

Lesieur, M. (1993). Turbulence in fluids., 412. https://doi.org/10.1115/1.3173656

Lindborg, E. (1999). Can the atmospheric kinetic energy spectrum be explained by two-dimensional turbulence? *Journal of Fluid Mechanics*, *388*, 259–288. https://doi.org/10.1017/S0022112099004851

Lindborg, E. (2007). Third-order structure function relations for quasi-geostrophic turbulence. *Journal of Fluid Mechanics*, *575*, 255–260. https://doi.org/10.1017/S0022112006003697

Liu, X., Xu, J., Gao, H., & Chen, G. (2009). Kelvin-Helmholtz billows and their effects on mean state during gravity wave propagation. *Annales Geophysicae*, *27*(7), 2789–2798. https://doi.org/10.5194/angeo-27-2789-2009

Lu, C., & Koch, S. E. (2008). Interaction of upper-tropospheric turbulence and gravity waves as obtained from spectral and structure function analyses. *Journal of the Atmospheric Sciences*, *65*(8), 2676–2690. https://doi.org/10.1175/2007JAS2660.1

Marshak, A., Davis, A., Wiscombe, W., & Cahalan, R. (1997). Scale invariance in liquid water distributions in marine stratocumulus. Part II: Multifractal properties and intermittency issues. *Journal of the Atmospheric Sciences*, *54*, 1423–1444. https://doi.org/10.1175/1520-0469(1997)054<1423:SIILWD>2.0.CO;2

Monin, A. S., & Yaglom, A. M. (1975). Statistical Fluid Mechanics: Mechanics of Turbulence, *2*, 874.

Nastrom, G. D., & Gage, K. S. (1985). A climatology of atmospheric wavenumber spectra of wind and temperature observed by commercial aircraft. *Journal of the Atmospheric Sciences*, *42*, 950–960. https://doi.org/10.1175/1520-0469(1985)042<0950:ACOAWS>2.0.CO;2

Nastrom, G. D., Gage, K. S., & Jasperson, W. H. (1984). Kinetic energy spectrum of large-and mesoscale atmospheric processes. *Nature*, *310*, 36–38. https://doi.org/10.1038/310036a0

Palmer, T. L., Fritts, D. C., & Andreassen, Ø. (1996). Evolution and breakdown of Kelvin-Helmholtz billows in stratified compressible flows. Part II: Instability structure, evolution, and energetics. *Journal of the Atmospheric Sciences*. https://doi.org/10.1175/1520-0469(1996)053<3192:EABOKB>2.0.CO;2

Smith, S. A., Fritts, D. C., & VanZandt, T. E. (1987). EVIDENCE FOR A SATURATED SPECTRUM OF ATMOSPHERIC GRAVITY WAVES. *Journal of the Atmospheric Sciences*, *44*, 1404–1410. https://doi.org/10.1175/1520-0469(1987)044<1404:EFASSO>2.0.CO;2

Xie, J.-H., & Bühler, O. (2019). Third-order structure functions for isotropic turbulence with bidirectional energy transfer. *Journal of Fluid Mechanics*, *877*, R3. https://doi.org/10.1017/jfm.2019.651

Yu, C. X., Gilmore, M., Peebles, W. A., & Rhodes, T. L. (2003). Structure function analysis of long-range correlations in plasma turbulence. *Physics of Plasmas*, *10*, 2772–2779. https://doi.org/10.1063/1.1583711